

PARKES RADIO SEARCHES OF *FERMI* GAMMA-RAY SOURCES AND MILLISECOND PULSAR DISCOVERIES

F. CAMILO¹, M. KERR², P. S. RAY³, S. M. RANSOM⁴, J. SARKISSIAN⁵, H. T. CROMARTIE⁶, S. JOHNSTON², J. E. REYNOLDS²,
M. T. WOLFF³, P. C. C. FREIRE⁷, B. BHATTACHARYYA⁸, E. C. FERRARA⁹, M. KEITH⁸, P. F. MICHELSON¹⁰,
P. M. SAZ PARKINSON^{11,12}, AND K. S. WOOD³

accepted for publication, July 15, 2015

ABSTRACT

In a search with the Parkes radio telescope of 56 unidentified *Fermi*-LAT gamma-ray sources, we have detected 11 millisecond pulsars (MSPs), 10 of them discoveries, of which five were reported in Kerr et al. (2012). We did not detect radio pulsations from another six pulsars now known in these sources. We describe the completed survey, which included multiple observations of many targets done to minimize the impact of interstellar scintillation, acceleration effects in binary systems, and eclipses. We consider that 23 of the 39 remaining sources may still be viable pulsar candidates. We present timing solutions and polarimetry for five of the MSPs, and gamma-ray pulsations for PSR J1903–7051 (pulsations for five others were reported in the second *Fermi*-LAT catalog of gamma-ray pulsars). Two of the new MSPs are isolated and five are in > 1 d circular orbits with $0.2\text{--}0.3 M_{\odot}$ presumed white dwarf companions. PSR J0955–6150, in a 24 d orbit with a $\approx 0.25 M_{\odot}$ companion but eccentricity of 0.11, belongs to a recently identified class of eccentric MSPs. PSR J1036–8317 is in an 8 hr binary with a $> 0.14 M_{\odot}$ companion that is probably a white dwarf. PSR J1946–5403 is in a 3 hr orbit with a $> 0.02 M_{\odot}$ companion with no evidence of radio eclipses.

Subject headings: gamma-rays: stars — pulsars: individual (PSR J0955–6150, PSR J1012–4235, PSR J1036–8317, PSR J1903–7051, PSR J1946–5403)

1. INTRODUCTION

The Large Area Telescope (LAT; Atwood et al. 2009) on the *Fermi Gamma-ray Space Telescope* is a superb instrument with which to study rotation-powered pulsars. Since mid-2008, it has been used to detect more than 170 pulsars at energies above 0.1 GeV (e.g., Abdo et al. 2010b)¹³. *Fermi* has identified millisecond pulsars (MSPs) as a ubiquitous class of gamma-ray sources (e.g., Abdo et al. 2009a). These old neutron stars, spun up by accretion from an evolved companion (Alpar et al. 1982), are a relatively local and isotropically distributed population, that make up only 10% of the identified population of pulsars in the Galactic disk. However, about half of known gamma-ray pulsars are MSPs.

Nearly half of the known gamma-ray MSPs were discov-

ered as radio objects in undirected (“all sky”) surveys prior to the launch of *Fermi*. Gamma-ray pulsations were subsequently detected with the aid of rotational ephemerides obtained from radio timing observations. Many slowly-rotating pulsars have been discovered via direct periodicity searches of sparse gamma-ray photons (e.g., Abdo et al. 2009b; Pletsch et al. 2012b), but so far this has not been possible unbiasedly for binary MSPs. However, the LAT has led to the discovery of MSPs in a different, and prolific, fashion. In the three LAT source catalogs (Abdo et al. 2010a; Nolan et al. 2012; Acero et al. 2015), there are hundreds of unidentified sources, many of which have spectral characteristics typical of pulsars. Radio searches of many of these have turned up dozens of MSPs so far, and once the radio ephemerides have been obtained, gamma-ray pulsations have almost always followed (e.g., Cognard et al. 2011; Barr et al. 2013).

Using the CSIRO Parkes telescope in 2009, we discovered five MSPs in a radio survey of 14 unidentified LAT sources (Kerr et al. 2012). In an extension of that survey we have discovered five more MSPs. Here we present the completed survey, and report on radio timing, polarimetric, and gamma-ray studies of some of the MSPs.

2. OBSERVATIONS, ANALYSIS, AND RESULTS

In this Section we describe the radio searches of unidentified gamma-ray sources that we performed at the Parkes telescope (Section 2.1), the sensitivity of the survey and relevant selection effects (Section 2.2), radio timing and polarimetric observations of the pulsars discovered (Sections 2.3 and 2.4), gamma-ray results for one of them (Section 2.5), and some X-ray observations (Section 2.6).

2.1. Parkes Radio Searches

2.1.1. Initial Searches of *IFGL* Sources

Keith et al. (2011) used a digital filterbank at Parkes to search 11 unidentified sources from the first *Fermi* LAT cat-

¹ Columbia Astrophysics Laboratory, Columbia University, New York, NY 10027, USA

² CSIRO Astronomy and Space Science, Australia Telescope National Facility, Epping, NSW 1710, Australia

³ Space Science Division, Naval Research Laboratory, Washington, DC 20375-5352, USA

⁴ National Radio Astronomy Observatory, Charlottesville, VA 22903, USA

⁵ CSIRO Parkes Observatory, Parkes, NSW 2870, Australia

⁶ Department of Astronomy, University of Virginia, Charlottesville, VA 22904-4325, USA

⁷ Max-Planck-Institut für Radioastronomie, D-53121 Bonn, Germany

⁸ Jodrell Bank Centre for Astrophysics, School of Physics and Astronomy, The University of Manchester, Manchester M13 9PL, UK

⁹ NASA Goddard Space Flight Center, Greenbelt, MD 20771, USA

¹⁰ W. W. Hansen Experimental Physics Laboratory, Kavli Institute for Particle Astrophysics and Cosmology, Department of Physics and SLAC National Accelerator Laboratory, Stanford University, Stanford, CA 94305, USA

¹¹ Santa Cruz Institute for Particle Physics, Department of Physics and Department of Astronomy and Astrophysics, University of California at Santa Cruz, Santa Cruz, CA 95064, USA

¹² Department of Physics, The University of Hong Kong, Pokfulam Road, Hong Kong, China

¹³ <https://confluence.slac.stanford.edu/display/GLAMCOG/Public+List+of+LAT-Detected+Gamma-Ray+Pulsars>.

alog (1FGL; Abdo et al. 2010a). Two MSPs and one slow pulsar were discovered in single observations of each target at a central frequency of 1.4 GHz. Subsequently, one of these MSPs was found to be associated with the corresponding LAT source.

At nearly the same time, in late 2009, we used an analog filterbank at Parkes to search 14 unidentified 1FGL sources (Kerr et al. 2012). The single observations of these targets resulted in the detection of six MSPs, five of them discoveries. However, confirmation of some of these MSPs was not easy: the search observations lasted for 1–2 hr each, but some of the pulsars were not detected in equivalent initial confirmation attempts, owing to the effects of interstellar scintillation. These and other selection effects (see Section 2.2 for details) led us to search some promising unidentified LAT sources repeatedly.

2.1.2. Repeated Searches of Unidentified LAT Sources

Our subsequent searches used the same equipment and methods as Kerr et al. (2012). In brief, total-power measures from the central beam of the 20 cm multibeam receiver were filtered into 512 contiguous 0.5 MHz-wide channels centered on 1390 MHz and sampled 8000 times per second, then digitized with 1-bit precision and written to disk for off-line analysis. Individual integration times were about 1 hr, and each LAT source was observed between one and nine times, depending on the then-perceived quality of the source and telescope availability (Table 1).

All the data were analyzed using PRESTO (Ransom 2001), which implements standard pulsar search techniques including radio-frequency interference excision and optimization for signals with changing apparent spin periods caused by orbital motion. Finite sampling time and smearing from dispersive propagation delays within finite-width filterbank channels both unavoidably degrade sensitivity to pulsed signals. Additional smearing can result from use of an incorrect dispersion measure (DM) to remove the delays between channels. We dedispersed each observation using a set of trial DMs such that this effect was negligible. This was done up to twice the maximum DM predicted by the Cordes & Lazio (2002) model for the corresponding line of sight (see Table 1). The maximum acceleration searched for corresponded to signals drifting by $\pm 200/n_h$ bins in the Fourier domain, where n_h is the largest harmonic at which a signal is detected (up to 16 harmonics were summed, in powers of two). This was parameterized by $z_{\max} = 200$ within PRESTO (Ransom et al. 2002).

In the 2009 searches (Section 2.1.1) we detected six MSPs in single observations of 14 LAT sources (Table 1, above the horizontal dividing line). In 2010–2011 we re-observed seven of the remaining eight 1FGL sources (Table 1, above the dividing line), but no new pulsars were detected¹⁴.

The 1FGL catalog was based on 11 months of LAT data. The 2FGL catalog (Nolan et al. 2012) was based on two years of data. In 2012 we selected new search targets, based on a three-year source list developed by the LAT collaboration but never published (the subsequent 3FGL catalog is based on four years of data and a different pipeline; Acero et al. 2015). As for the 1FGL searches (Kerr et al. 2012), we restricted ourselves to non-variable southern sources with no

plausible known blazar counterparts and with a LAT positional uncertainty (95% confidence level error radius) $\leq 7'$, to fit within the 1.4 GHz primary beam of the Parkes telescope. The remaining sources were classified by visual inspection of the gamma-ray spectral energy distribution to pick out candidates with spectral shape resembling those of known pulsars, which typically have exponentially cut-off power-law spectra (Abdo et al. 2013). Spectral modeling and source localization is more difficult for LAT sources near the Galactic plane, and we only considered those with $|b| > 4^\circ$.

The new target set consisted of 49 sources, each observed between one and seven times, for 122 integrations in the aggregate. Seven of the 49 targets had also been observed in their prior 1FGL incarnation (italicized in Table 1). Among the remaining 42, we discovered five MSPs (Table 1).

Overall, we searched 56 individual LAT sources in our Parkes survey using the analog filterbank system. We detected 11 MSPs, of which 10 were discoveries (Table 1). In fact, radio and/or gamma-ray pulsars are now known in 17 of those 56 sources (Table 2). We discuss the sources, in particular which might still be good pulsar candidates, in Section 3.

Three of the five new MSPs were detected unbiasedly in all their search observations (i.e., without prior knowledge of their DM or approximate spin period). However, PSR J1946–5403 was detected in only three of six observations, and PSR J1036–8317 was detected in only the third of three search observations. We now consider the reasons behind these failures to consistently detect some new pulsars.

2.2. Sensitivity and Selection Effects

The nominal sensitivity of our survey to a $P = 2$ ms pulsar with a duty cycle of 25% and $DM \lesssim 40$ pc cm⁻³, for a typical integration time of 1 hr (Table 1), and for a sky temperature corresponding to the average at the locations of the targets searched, was 0.2 mJy — provided that the dilution of power in the Fourier domain caused by orbital motion in a putative binary was ideally corrected by our acceleration search analysis. However, two of the newly discovered MSPs have orbital periods P_b such that the discovery integrations were 0.1–0.3 P_b (Section 2.3), for which this idealized correction breaks down badly; how badly, for a given system, depends on the observed orbital phases (see Figure 1, and Johnston & Kulkarni 1991; Bagchi et al. 2013).

As well, a considerable fraction of LAT-selected MSPs is in eclipsing binary systems (e.g., Hessels et al. 2011). Multiple observations of a promising source can thus help combat these factors affecting detectability. In addition, the flux density received from many MSPs is severely affected by interstellar scintillation (see, e.g., Figure 1 of Levin et al. 2013). As we now show, this has played a very significant role in our survey, and the early realization of the magnitude of some of these selection effects is what led us to do multiple observations of many unidentified LAT sources starting in 2010 (Section 2.1.2).

2.2.1. Interstellar Scintillation and Detection Statistics

In order to acquire the detections required to determine the timing solution for PSR J1514–4946 (Section 2.3), we used 100 hr of Parkes telescope time in 79 observations on 54 days spread over 2 yr. In only 27 of those observations did we detect the pulsar in a *relatively* unbiased manner — by dedispersing the raw data using the known DM, performing an acceleration search, and looking for a signal with period

¹⁴ One of these sources is now known to harbor PSR J1227–4853, which recently transitioned to a radio-emitting state (Roy et al. 2015, and see Table 2).

Table 1
Radio Searches of FGL Sources at Parkes: Observations

Name ^a	R.A. ^b (J2000.0)	Decl. ^b (J2000.0)	<i>l</i> (deg)	<i>b</i> (deg)	Integration time (min)	DM _{max} ^c (pc cm ⁻³)
3FGL J0101.0–6422	01 ^h 00 ^m 58 ^s	−64° 24′ 06″	301.2	−52.7	60	270
3FGL J0602.8–4016	06 ^h 03 ^m 05 ^s	−40° 11′ 04″	246.8	−25.9	90, 120	270
<i>3FGL J0933.9–6232</i>	09 ^h 34 ^m 00 ^s	−62° 30′ 17″	282.2	−7.8	120, 60, 60, 60, 60	435
<i>3FGL J1035.7–6720</i>	10 ^h 36 ^m 10 ^s	−67° 21′ 05″	290.4	−7.8	120, 86, 136, 60, 60, 60	435
<i>3FGL J1227.9–4854</i>	12 ^h 27 ^m 50 ^s	−48° 51′ 57″	298.9	13.8	120, 65, 60	307
<i>3FGL J1231.6–5113</i>	12 ^h 31 ^m 49 ^s	−51° 18′ 49″	299.8	11.4	120	270
3FGL J1514.2–4947	15 ^h 14 ^m 06 ^s	−49° 45′ 33″	325.2	6.8	120	270
<i>3FGL J1624.2–4041</i>	16 ^h 24 ^m 07 ^s	−40° 41′ 20″	340.6	6.2	120, 120, 120, 60, 60, 60	435
3FGL J1658.4–5323	16 ^h 58 ^m 43 ^s	−53° 17′ 43″	335.0	−6.6	83	270
<i>3FGL J1744.1–7619</i>	17 ^h 44 ^m 02 ^s	−76° 20′ 25″	317.1	−22.5	41, 90, 80, 72, 71, 78, 60, 60, 60	192
3FGL J1747.6–4037	17 ^h 47 ^m 29 ^s	−40° 36′ 07″	350.2	−6.4	86	270
3FGL J1902.0–5107	19 ^h 02 ^m 05 ^s	−51° 09′ 45″	345.6	−22.4	70	270
<i>3FGL J2039.6–5618</i>	20 ^h 39 ^m 30 ^s	−56° 20′ 45″	341.2	−37.1	75, 112, 60	270
3FGL J2241.6–5237^d	22 ^h 41 ^m 52 ^s	−52° 37′ 38″	337.4	−54.9	120	270
3FGL J0133.0–4413	01 ^h 33 ^m 27 ^s	−44° 08′ 29″	279.2	−71.0	60, 60, 60, 60, 60, 60	77
3FGL J0216.1–7016	02 ^h 14 ^m 04 ^s	−69° 52′ 06″	292.9	−45.6	60	115
3FGL J0744.8–4028	07 ^h 44 ^m 59 ^s	−40° 29′ 49″	254.6	−8.0	60	717
3FGL J0802.3–5610	08 ^h 02 ^m 46 ^s	−56° 15′ 32″	270.0	−13.2	60, 60, 35, 35, 35	627
3FGL J0933.9–6232	09 ^h 34 ^m 02 ^s	−62° 31′ 34″	282.2	−7.9	60, 35	627
3FGL J0940.6–7609	09 ^h 40 ^m 45 ^s	−76° 09′ 34″	292.2	−17.4	60	269
3FGL J0940.7–6102	09 ^h 40 ^m 57 ^s	−61° 05′ 10″	281.9	−6.3	60	653
3FGL J0954.8–3948	09 ^h 55 ^m 03 ^s	−39° 49′ 25″	269.9	11.5	60, 60, 60, 60, 60	371
3FGL J0955.6–6148	09 ^h 55 ^m 39 ^s	−61° 48′ 36″	283.7	−5.7	60, 60	653
3FGL J1012.0–4235	10 ^h 12 ^m 07 ^s	−42° 35′ 01″	274.2	11.2	60	371
3FGL J1025.1–6507	10 ^h 25 ^m 00 ^s	−65° 07′ 22″	288.3	−6.5	60	755
3FGL J1035.7–6720	10 ^h 36 ^m 09 ^s	−67° 22′ 17″	290.4	−7.8	45, 60, 60	563
3FGL J1036.0–8317	10 ^h 36 ^m 20 ^s	−83° 17′ 01″	298.9	−21.5	60, 60, 60	192
3FGL J1057.7–6624	10 ^h 58 ^m 43 ^s	−66° 21′ 59″	292.0	−5.9	60, 60, 60, 60	755
3FGL J1136.6–6826	11 ^h 36 ^m 47 ^s	−68° 25′ 37″	296.1	−6.5	60	755
3FGL J1227.9–4854	12 ^h 27 ^m 42 ^s	−48° 53′ 28″	298.9	13.8	60, 60	371
3FGL J1231.6–5113	12 ^h 31 ^m 34 ^s	−51° 12′ 31″	299.8	11.5	60	435
3FGL J1238.3–4543	12 ^h 38 ^m 19 ^s	−45° 43′ 18″	300.5	17.1	60	269
3FGL J1306.8–4031	13 ^h 06 ^m 52 ^s	−40° 32′ 35″	306.1	22.2	60	192
3FGL J1311.8–3430	13 ^h 11 ^m 46 ^s	−34° 29′ 19″	307.7	28.2	60, 58, 60, 58	154
3FGL J1325.2–5411	13 ^h 25 ^m 15 ^s	−54° 11′ 13″	307.9	8.4	60	627
3FGL J1326.7–4727	13 ^h 26 ^m 40 ^s	−47° 27′ 52″	309.1	15.0	60, 60	371
3FGL J1417.5–4402	14 ^h 17 ^m 30 ^s	−44° 02′ 40″	318.9	16.1	60	307
3FGL J1417.7–5026	14 ^h 17 ^m 39 ^s	−50° 25′ 33″	316.7	10.1	60	627
3FGL J1518.2–5232	15 ^h 18 ^m 27 ^s	−52° 33′ 57″	324.3	4.1	60, 60, 60, 60	1044
3FGL J1536.3–4949	15 ^h 36 ^m 29 ^s	−49° 49′ 45″	328.2	4.8	37, 37, 16, 60, 60, 60	883
3FGL J1539.2–3324	15 ^h 39 ^m 15 ^s	−33° 25′ 42″	338.7	17.5	60, 15, 52, 60	269
3FGL J1603.7–6011	16 ^h 03 ^m 44 ^s	−60° 11′ 12″	324.8	−5.7	60	883
3FGL J1617.4–5846	16 ^h 17 ^m 28 ^s	−58° 46′ 19″	327.0	−5.9	60	883
3FGL J1624.2–4041	16 ^h 24 ^m 09 ^s	−40° 40′ 23″	340.6	6.2	60, 60	883
3FGL J1702.8–5656	17 ^h 02 ^m 33 ^s	−56° 54′ 54″	332.4	−9.2	60, 60, 60, 60	627
3FGL J1717.4–5157	17 ^h 17 ^m 35 ^s	−51° 57′ 58″	337.7	−8.1	60	755
3FGL J1736.2–4444	17 ^h 36 ^m 13 ^s	−44° 44′ 50″	345.5	−6.7	60	883
3FGL J1744.1–7619	17 ^h 44 ^m 11 ^s	−76° 20′ 29″	317.1	−22.5	60	192
3FGL J1753.6–4447	17 ^h 53 ^m 38 ^s	−44° 47′ 50″	347.1	−9.4	60	627
3FGL J1803.3–6706	18 ^h 03 ^m 25 ^s	−67° 07′ 14″	326.9	−20.4	60	230
3FGL J1808.3–3357	18 ^h 08 ^m 22 ^s	−33° 56′ 05″	358.1	−6.7	56, 60, 60, 60	755
3FGL J1831.6–6503	18 ^h 31 ^m 45 ^s	−65° 05′ 19″	329.9	−22.4	60	192
3FGL J1903.6–7052	19 ^h 02 ^m 43 ^s	−70° 53′ 49″	324.3	−26.4	60	269
3FGL J1946.4–5403	19 ^h 46 ^m 24 ^s	−54° 02′ 46″	343.9	−29.6	60, 60, 60, 60, 60, 54	154
3FGL J1959.8–4725	19 ^h 59 ^m 57 ^s	−47° 26′ 32″	351.8	−30.9	58, 60, 60, 35, 60	307
3FGL J2039.6–5618	20 ^h 39 ^m 51 ^s	−56° 20′ 26″	341.2	−37.2	60, 60, 60, 60	115
3FGL J2043.8–4801	20 ^h 43 ^m 49 ^s	−48° 00′ 45″	351.7	−38.3	60, 60	115
3FGL J2112.5–3044	21 ^h 12 ^m 36 ^s	−30° 42′ 37″	14.9	−42.4	56, 60, 60, 60, 60, 60	103
3FGL J2131.1–6625	21 ^h 31 ^m 06 ^s	−66° 24′ 42″	326.7	−40.3	60, 60	115
3FGL J2133.0–6433	21 ^h 33 ^m 30 ^s	−64° 31′ 58″	328.7	−41.3	60, 60, 60, 60, 60, 60	103
3FGL J2200.0–6930	22 ^h 00 ^m 00 ^s	−69° 31′ 37″	321.3	−40.9	60	115
3FGL J2220.6–6833	22 ^h 20 ^m 24 ^s	−68° 32′ 22″	320.8	−43.0	60, 60, 60	115
3FGL J2333.0–5525	23 ^h 33 ^m 04 ^s	−55° 25′ 32″	324.2	−58.3	60, 60	87

Note. — Boldfaced entries denote observations with detection of MSPs. Discoveries in single-observation searches of the first 14 entries (listed above the horizontal line) were reported in Kerr et al. (2012). Italicized entries denote sources re-observed in 2012 at the improved locations listed below the horizontal line.

^a The names given are of the 3FGL sources closest to our pointing locations (the offset between the pointing positions given here and the 3FGL positions are provided in Table 2).

^b Parkes telescope pointing position.

^c Maximum trial dispersion measure used in our analysis of the respective data set(s), corresponding approximately to twice the maximum DM predicted by the Cordes & Lazio (2002) model for the corresponding line of sight. The first observation of each source above the horizontal line was analyzed with DM_{max} = 270 pc cm⁻³ (Kerr et al. 2012).

^d MSP discovered independently by Keith et al. (2011).

Table 2
Radio Searches of FGL Sources at Parkes: Source Information

3FGL name ^a	$\Delta\theta^b$ (deg)	r95 ^c (deg)	Class ^d	Sig ^e (σ)	Curve ^f (σ)	Var ^g	Spectrum notes ^h	N_{obs}^i
J0101.0–6422^j	0.03	0.04	PSR	26.8	6.8	55	1 CpR	1
J0133.0–4443	0.12	0.09	bll	7.7	0.5	48	4 lhr	6
J0216.1–7016	0.44	0.12	bcu	6.0	0.5	49	4 ld	1
J0602.8–4016	0.10	0.04	bcu	15.3	1.8	49	4 lih	2
J0744.8–4028	0.04	0.08	bcu	7.4	1.9	39	3 ld	1
J0802.3–5610	0.11	0.10		12.3	3.6	44	4 ld	5
J0933.9–6232	0.01	0.04		22.0	8.8	59	1 CPr	2
J0940.6–7609	0.01	0.10		10.0	1.1	48	3 ld	1
J0940.7–6102	0.05	0.21	bcu	6.4	2.7	51	3 pr	1
J0954.8–3948	0.04	0.09		18.8	3.9	51	3 D*	5
J0955.6–6148^k	0.00	0.11	psr	7.0	2.2	39	2 cr	2
J1012.0–4235^k	0.02	0.07	psr	8.8	3.6	38	3 ?pr	1
J1025.1–6507	0.02	0.09		7.3	2.7	52	3 ld	1
J1035.7–6720^l	0.06	0.04		30.4	8.3	47	1 CpR	3
J1036.0–8317^k	0.01	0.12	psr	6.6	2.3	42	3 ?p	3
J1057.7–6624	0.10	0.06		9.1	1.2	29	4 LD	4
J1136.6–6826	0.01	0.11	bcu	7.7	0.7	43	4 LD	1
J1227.9–4854^m	0.04	0.04	psr	38.6	4.6	74	3 Dh*	2
J1231.6–5113	0.01	0.11		13.4	5.6	46	1 CPr	1
J1238.3–4543	0.01	0.08	bcu	8.0	0.3	61	4 ?lh	1
J1306.8–4031	0.01	0.07		14.9	0.3	43	4 ID	1
J1311.8–3430ⁿ	0.02	0.02	PSR	62.3	9.0	52	1 CR	4
J1325.2–5411	0.00	0.10		7.0	2.5	31	3 ?ld	1
J1326.7–4727	0.02	0.05	glc	11.3	6.1	66	1 Cpr	2
J1417.5–4402	0.00	0.06		12.5	1.4	54	2 cd	1
J1417.7–5026	0.02	0.11		6.1	0.4	40	4 Ld	1
J1514.2–4947^j	0.03	0.02	PSR	39.4	9.3	35	1 CpR	1
J1518.2–5232	0.04	0.07		10.3	3.6	62	2 cr	4
J1536.3–4949^o	0.02	0.02	psr	60.0	8.5	51	3 pRh	6
J1539.2–3324	0.02	0.04		19.2	9.6	57	2 cPr	4
J1603.7–6011	0.01	0.09		5.0	3.6	50	4 ?h	1
J1617.4–5846	0.00	0.08	fsrq	15.8	1.6	128	5 LDV	1
J1624.2–4041^l	0.02	0.04		19.2	7.3	50	1 cpR	2
J1658.4–5323^j	0.10	0.06	PSR	16.9	6.5	38	1 Cr	1
J1702.8–5656	0.05	0.04		28.8	6.1	58	3 rdh*	4
J1717.4–5157	0.02	0.09	fsrq	12.2	2.5	383	5 LDV	1
J1736.2–4444	0.00	0.05	glc	16.9	3.3	46	2 cd	1
J1744.1–7619^l	0.01	0.03		32.8	9.9	51	1 CPR	1
J1747.6–4037^j	0.05	0.07	PSR	10.0	2.8	46	2 ?c	1
J1753.6–4447	0.01	0.08		11.1	4.0	41	1 cpr	1
J1803.3–6706	0.01	0.08		10.4	1.8	43	3 ldh	1
J1808.3–3357	0.03	0.09		8.7	4.4	50	1 cpr	4
J1831.6–6503	0.02	0.10		8.5	4.5	35	2 cPr	1
J1902.0–5107^j	0.04	0.04	PSR	28.9	6.2	50	1 CR	1
J1903.6–7052^k	0.08	0.05	PSR	16.3	1.9	52	2 cd	1
J1946.4–5403^k	0.01	0.06		20.2	6.8	39	1 pr	6
J1959.8–4725	0.02	0.03	bcu	19.2	3.9	49	4 pihr	5
J2039.6–5618	0.04	0.04		25.3	5.1	34	1 CpR	4
J2043.8–4801	0.01	0.08		9.5	3.0	35	2 cr	2
J2112.5–3044	0.02	0.04		30.1	7.6	51	1 CpR	6
J2131.1–6625	0.01	0.11		10.1	3.1	52	2 rl	2
J2133.0–6433	0.05	0.10		10.1	4.7	49	2 Pr	7
J2200.0–6930	0.02	0.13		9.5	0.6	41	3 ld	1
J2220.6–6833	0.02	0.11		5.7	1.1	50	4 lh	3
J2241.6–5237^p	0.03	0.03	PSR	51.7	12.6	60	1 CpR	1
J2333.0–5525	0.00	0.08		10.7	2.5	42	2 cr	2

^a Boldfaced names denote 17 3FGL sources with now known associated radio and/or gamma-ray pulsars; struck-through names indicate 16 sources that we believe are no longer viable pulsar candidates (see next-to-last column).

^b Offset between 3FGL position and pointing position in Table 1 (where there are two of the latter, only the second is listed here); the Parkes beam half-width at half-maximum is 0.12°.

^c Size of 3FGL source error box (95% confidence level semi-major axis; all 3FGL properties listed here are taken from the 3FGL catalog, Acero et al. 2015).

^d Classification from 3FGL pipeline. “PSR” is a pulsar with LAT pulsations; “psr” is a positionally coincident pulsar so far without LAT pulsations; “bll” is a BL Lac; “bcu” is an unclassified blazar; “glc” is a globular cluster; “fsrq” is a flat-spectrum radio quasar.

^e 3FGL source significance.

^f Significance of curvature of 3FGL source spectrum when fit to a log-parabolic model.

^g Variability index of source (> 73 indicates variability at the > 99% C.L.).

^h See Section 3.5 for a description of these classifications and characteristics.

ⁱ Number of observations of each target at position closest to 3FGL source (from Table 1), $\Delta\theta$ offset from it.

^j Radio MSP discoveries from our Parkes survey, first reported in Kerr et al. (2012).

^k First reported in this work.

^l Pulsar discovered via gamma-ray pulsations (H. J. Pleisch, private communication).

^m Intermittently radio-emitting MSP (Roy et al. 2015).

ⁿ MSP in 93-minute orbit discovered via gamma-ray pulsations (Pleisch et al. 2012a), subsequently detected at the GBT (Ray et al. 2013).

^o Radio MSP discovered at the GMRT (Ray et al. 2012).

^p Radio and gamma-ray MSP, discovered at Parkes (Keith et al. 2011).

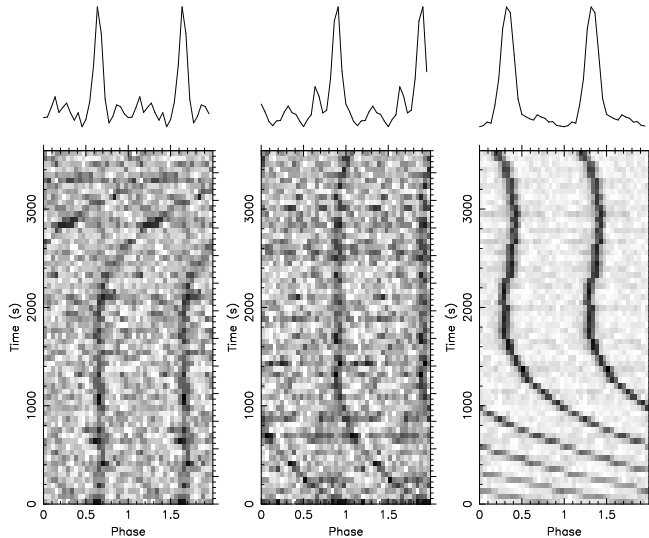


Figure 1. Pulse profiles (repeated twice) as a function of time during the 1 hr observation times, and integrated (at top), for each of the three unbiased detections of PSR J1946–5403, folded according to the best values of spin period and period derivative determined by the search software. In the other three search observations of this source (Table 1) the pulsar was not detected unbiasedly, because of the dilution of power in the Fourier domain caused by the rapid non-linear change in projected orbital velocity for this 3 hr binary system. A constant-acceleration search such as the ones we performed cannot correct for this effect well enough.

3.589 ms. In several of those observations the pulsar was not detectable without prior knowledge of the DM and approximate period. A pulsar like PSR J1514–4946 is therefore discoverable in a search like ours at Parkes less than 1/3 of the time! This is due to its small intrinsic flux density combined with very large modulation owing to propagation through the dynamic and inhomogeneous interstellar medium (see Figure 2).

This large modulation of observed flux density is primarily caused by strong diffractive interstellar scintillation. This causes the detected pulsar signal strength in the time–frequency plane to form patches (or “scintles”) of characteristic size $\Delta\nu$ and Δt . For a given observing frequency, $\Delta\nu$ increases strongly with decreasing pulsar distance d , while Δt increases particularly with decreasing pulsar velocity in the plane of the sky V_{\perp} (see, e.g., Johnston et al. 1998; Nicastro et al. 2001; Lorimer & Kramer 2005). When $\Delta\nu$ or Δt are large compared to the observing bandwidth and integration time, deep fluctuations in observed flux density result. While we have not measured $\Delta\nu$ or Δt for PSR J1514–4946, the observations (e.g., Figure 2) are consistent with large values for both (e.g., $\gtrsim 100$ MHz and $\gtrsim 1$ hr, respectively), accounting for the very large observed modulations.

The measured flux density of PSR J1658–5324 is affected by scintillation even more, ranging over a factor > 50 . It was detected in a relatively unbiased manner only 70% of the time, and less than 1/2 of the time in the absence of prior DM and period information. PSR J0101–6422, another MSP discovered in the first phase of our survey, for which we have good statistics, is detectable 80% of the time (Kerr et al. 2012). These detection statistics are based on typical 1 hr individual Parkes timing observations (Section 2.3).

For PSR J1903–7051, the observed flux densities range over a factor > 10 . PSR J1902–5105 varies less: its recorded flux density has a standard deviation of 40% of the mean.

These MSPs are reasonably bright, with relatively narrow pulse profiles, and were always detected in typical 20 min Parkes timing observations. For PSR J1747–4036, with a large DM = 153 pc cm^{−3}, the effects of scintillation modulate the flux density that we record by only 25% about the mean, and it was detected 100% of the time at Parkes and the GBT (Section 2.3).

Away from the Galactic plane, putative pulsar counterparts to unidentified gamma-ray sources are largely expected to be relatively nearby MSPs, which as a class have relatively small space velocities (e.g., Gonzalez et al. 2011). Depending on observing parameters (frequency, bandwidth, and integration time), these characteristics can make them particularly susceptible to deep flux density fluctuations, in turn with important implications for radio searches. Scintillation modulations in the strong regime have exponential statistics (e.g., Rickett 1990), with median flux density measurements less than the mean. Two of the six MSPs for which we have already obtained timing solutions (Section 2.3) display flux densities that vary by a factor of > 40 , with small median values and, given scintillation statistics, not detectable in an unbiased manner most of the time for the parameters of our Parkes survey.

The foregoing strongly suggests that an unidentified LAT source that is a good pulsar candidate should be searched repeatedly before much of a statement can be made about the likelihood of it being a radio MSP beaming towards the Earth. Eight of the 10 MSPs that we discovered were detected on their first observations (Table 1), but as the preceding account illustrates, in some cases (particularly for PSRs J1514–4946 and J1658–5324) this was fortuitous. Based on our empirical evidence, we judge that every promising LAT source should be observed a *minimum* of three or four times in a survey such as the one we did at Parkes before it can reasonably be considered searched in an average sense.

As indicated in Table 2, we consider that a number of our survey targets remain promising pulsar candidates, and at least some should be re-searched in radio. We discuss this more in Sections 3.5 and 3.6.

2.3. Radio Timing

We began timing observations of all 10 MSPs immediately following their discovery. In Table 3 we present initial parameters for the four most recent discoveries. We have determined phase-connected rotational ephemerides for the six remaining MSPs. That for PSR J0101–6422 was reported in Kerr et al. (2012); the other five are given in Tables 4 and 5, which also list available flux density measurements.

PSR J1747–4036 was observed mainly at the NRAO Green Bank Telescope (GBT), using the GUPPI spectrometer¹⁵ to sample a bandwidth of 800 MHz centered at 2 GHz, with typical integration times of 5 min.

The remaining MSPs were observed exclusively at Parkes where we first used the analog filterbank/PMDAQ data acquisition system as employed in the discovery observations, and later a digital filterbank (PDFB3/4), in all cases centered at 1.4 GHz. Each observation typically lasted for 1 hr, except for the brighter PSRs J1902–5105 and J1903–7051 (about 20 min). Apart from a dense set of observations to obtain orbital parameters for the binary pulsars, and to unambiguously establish pulse numbering, we aimed to detect each pulsar approximately monthly over a span of 1–2 yr. Especially for

¹⁵ <https://safe.nrao.edu/wiki/bin/view/CICADA/GUPPIUsersGuide>.

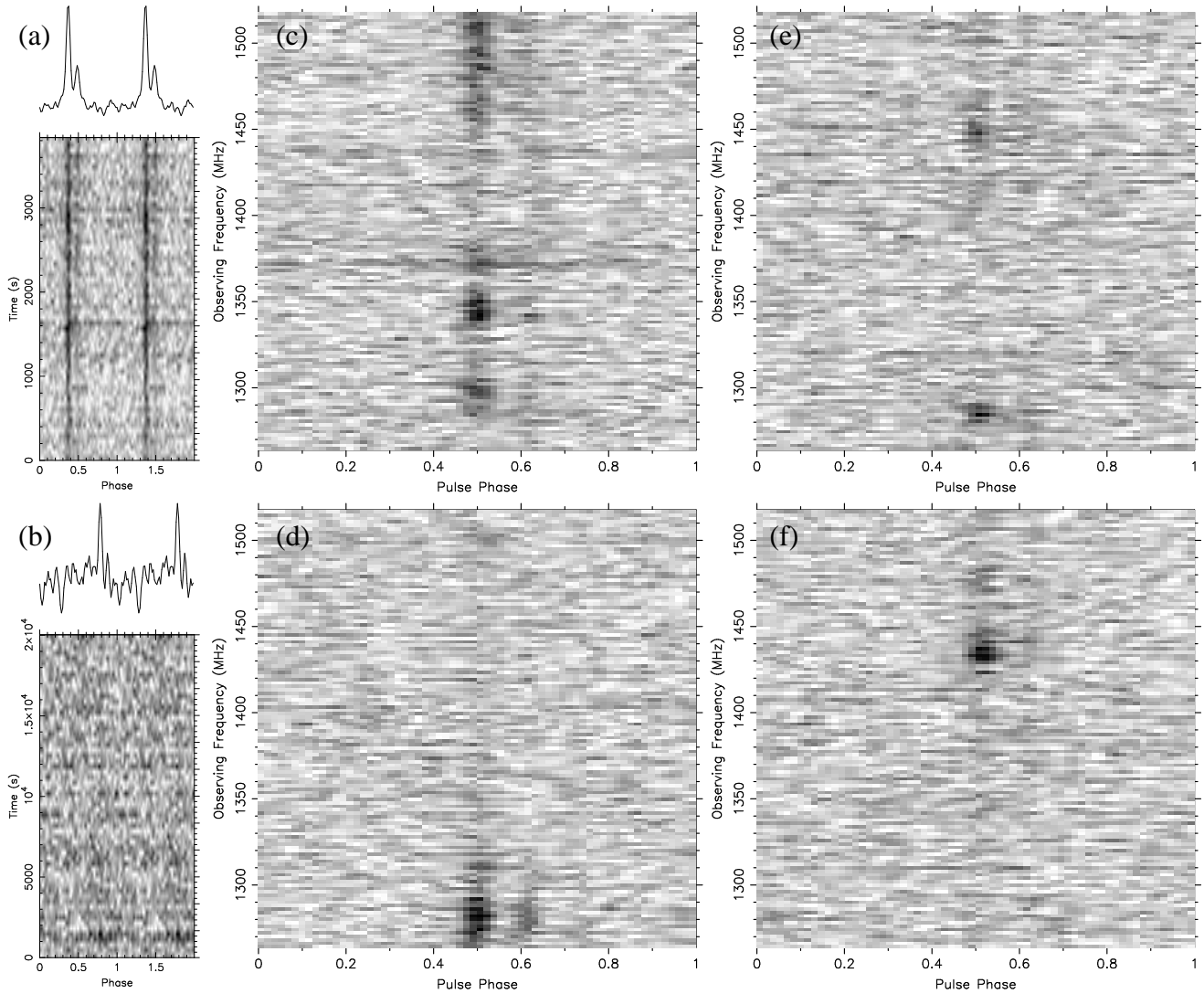


Figure 2. PSR J1514–4946 and its variable flux density due to scintillation in the ISM, observed at Parkes at 1.4 GHz with 256 MHz of bandwidth using the analog filterbank system. All profiles are shown with 64 phase bins per period ($P = 3.6$ ms), with a linear greyscale, and with arbitrary phases between plots. (a) The best detection among 79 observations spanning 2 years, showing the signal strength gently increasing during the observation, with the integrated profile at the top. (b) An extremely weak detection, obtained only by folding 6 hr of data modulo the period predicted from the timing solution. (c) Signal strength as a function of radio frequency for the observation also shown in (a). (d) A 0.7 hr good detection with average flux density half of that shown in (a) and (c), and with very different time-integrated frequency structure. (e, f) Two observations separated by 9 hr (of length 1.0 hr and 1.2 hr, respectively), showing very different frequency structure. In many instances, one or two features of ≈ 10 MHz in width dominate the detected signal. Often, no such feature is present and the pulsar is extremely faint, or not detectable.

PSR J1514–4946, this required a very large number of observations, because the pulsar is very faint on average and its received radio flux density varies enormously due to interstellar scintillation (Section 2.2.1). We improved the precision of the timing solutions by substantially extending the measurement baselines with a few additional observations in 2014 and early 2015.

We used the PRESTO and PSRCHIVE (Hotan et al. 2004) software to analyze the raw data and obtain pulse times-of-arrival (TOAs). For the MSPs with sparse radio detections, we obtained initial estimates of the orbital parameters using the method described in Freire et al. (2001). We then used TEMPO¹⁶ and TEMPO2 (Hobbs et al. 2006) to obtain phase-connected timing solutions. Starting with solutions spanning ≈ 1 yr for each pulsar, we detected gamma-ray pulsations for

¹⁶ <http://tempo.sourceforge.net>.

six MSPs. For PSR J1903–7051 we then obtained a few LAT TOAs. While the radio TOAs have much higher precision, they span only 3 yr. Adding gamma-ray TOAs increases the solution span and improves some results, in particular the proper motion measurement (see Section 2.5.2).

2.4. Polarimetry

In principle, study of the polarized radio emission from pulsars can constrain the magnetic field geometry and, particularly when considered together with gamma-ray profile characteristics, can elucidate emission locations and mechanisms (cf. Section 3.2).

In order to measure the polarization characteristics of each pulsar, we used the digital filterbank PDFB3 at Parkes, and GUPPI at GBT in coherent dedispersion mode, to do a few observations recording calibrated folded full-Stokes pulse profiles. These data were analyzed in standard fashion with

Table 3
Preliminary Parameters for Four Millisecond Pulsars

	PSR J0955–6150	PSR J1012–4235	PSR J1036–8317	PSR J1946–5403
Right ascension ^a , R.A. (J2000.0)...	09 ^h 55 ^m 39 ^s	10 ^h 12 ^m 07 ^s	10 ^h 36 ^m 20 ^s	19 ^h 46 ^m 24 ^s
Declination ^a , decl. (J2000.0)	–61°48′36″	–42°35′01″	–83°17′01″	–54°02′46″
Spin period, P (ms)	1.999	3.101	3.408	2.710
Dispersion measure, DM (pc cm ^{–3})	160.7	71.6	27.0	23.7
Orbital period, P_b (d)	24.578	37.972	0.335	0.130
Projected semi-major axis, x (l-s) .	13.283	21.263	0.506	0.0435
Eccentricity, e	0.11	< 0.001	< 0.001	< 0.001
Companion mass ^b , m_2 (M_\odot)	> 0.21	> 0.26	> 0.14	> 0.021
Galactic longitude, l (deg)	283.7	274.2	298.9	343.9
Galactic latitude, b (deg)	–5.7	11.2	–21.5	–29.6
DM-derived distance ^c , d (kpc)	3.8	2.5	1.0	0.9

Note. — The listed P and DM values are from the discovery observations. Orbital parameters are from fits to sets of Doppler-shifted barycentered periods.

^a These discovery pointing positions have $\pm 7'$ uncertainties. On the assumption that the MSPs are associated with the target gamma-ray sources, in some cases the position is better constrained (see Table 2).

^b Derived from the pulsar mass function f_1 assuming $m_1 = 1.35 M_\odot$ (Thorsett & Chakrabarty 1999) and $i < 90^\circ$. $f_1 = x^3(2\pi/P_b)^2 T_\odot^{-1} = (m_2 \sin i)^3 / (m_1 + m_2)^2$, where $T_\odot \equiv GM_\odot/c^3 = 4.925 \mu\text{s}$, m_1 and m_2 are the pulsar and companion masses, respectively, and i is the orbital inclination angle.

^c Using the Cordes & Lazio (2002) Galactic free electron density model. The individual estimates have substantial uncertainties.

PSRCHIVE. The resulting profiles are shown in Figures 3 and 4, and rotation measures (RMs) are listed in Tables 4 and 5.

The main profile component of PSR J1514–4946 is about 80% linearly polarized, with a flat position angle (P.A.) of linear polarization (Figure 3a).

PSR J1658–5324 has a complex profile, with a high (up to 100%) linear polarization fraction in most pulse components (Figure 3b). Such a high level of linear polarization is relatively uncommon among MSPs (see Yan et al. 2011; Dai et al. 2015). Despite the P.A. being measured over a large span of rotation phase, we were not able to obtain a satisfactory rotating vector model fit (Radhakrishnan & Cooke 1969).

The profile of PSR J1747–4036 is curious. This MSP has the second largest value of DM/ P among those known in the Galactic disk, and so was particularly well-suited for observing with a coherent dedispersion system. We show two such observations in Figure 3c. At 1.5 GHz, the profile has two featureless components, with a very flat P.A. throughout. Lack of variation in P.A. across the entire profile is unusual (there is no such example in a well-studied sample of 24 MSPs; Dai et al. 2015). The profile observed at 2 GHz (which overlaps in frequency with that at 1.5 GHz) looks similar. At 0.8 GHz, however (bottom panels of Figure 3c), the second component is brighter than the first, signifying that it has a steeper spectrum, and a third component appears (more easily discernible in linear polarization), with P.A.s offset by about 90° from the rest of the profile. At this frequency, emission is detectable across 85% of the pulse period (but the observed profile may be somewhat affected by multi-path propagation; Cordes & Lazio 2002 predict pulse broadening of $0.02P$).

The PSR J1902–5105 profile is relatively unusual in showing no discernible linear polarization (there is possibly a very small amount of circular polarization in both principal components; Figure 3d).

The radio profile of PSR J1903–7051 is shown in the bottom panel of Figure 4. It displays a weak, highly-polarized component (pulse phase $\phi \approx 0.58$) leading a much stronger double-peaked component ($0.65 \lesssim \phi \lesssim 0.85$). The first peak is highly linearly polarized and also shows a degree of circular polarization, while the trailing (brightest) peak is completely unpolarized.

2.5. Gamma-ray Observations and Analysis

The gamma-ray properties of the first five MSPs we discovered (PSR J0101–6422 and those in Table 4) have been reported elsewhere (Kerr et al. 2012; Abdo et al. 2013), and we focus here on the newly-detected gamma-ray pulsations of PSR J1903–7051. To characterize its properties, we analyzed “reprocessed Pass 7” SOURCE class *Fermi*-LAT events collected between 2008 August 4 (the start of nominal operations) and 2015 February 1, and with energies between 0.1 and 30 GeV. The data were filtered to exclude events whose reconstructed direction exceeds a zenith angle of 100° and those taken when the observatory was rocked more than 52° from the zenith, or when the region of interest (ROI) around the pulsar approached the Earth’s limb. These cuts minimize the bright gamma-ray background contribution from the limb of the Earth.

2.5.1. Spectral Analysis and Photon Weights

We considered a $20^\circ \times 20^\circ$ region around PSR J1903–7051, and used the binned likelihood formulation of *glike* (*Fermi* Science Tools v. 09-35-02¹⁷) to fit an exponentially cut-off power law to the pulsar emission, $dN/dE = N_0(E/E_0)^{-\Gamma} \exp(-E/E_c)$. We used the P7REP_SOURCE_V15 model of the instrument response functions¹⁸ and the isotropic and diffuse background models of the 3FGL catalog (Acero et al. 2015), as well as the point sources therein. The best-fit parameters and their error estimates are listed in the last section of Table 5. With models for the pulsar and background sources, we can compute a weight w_i for each photon i giving the probability that the photon originated from the pulsar (Kerr 2011a). These weights allow improved separation of the pulsar signal from its background in the following analyses.

2.5.2. Pulsar Timing

Folding LAT data for PSR J1903–7051 based on the radio-only timing solution results in a clear drift in the position of the gamma-ray profile peak outside the time interval covered by the radio ephemeris. Thus, using the same selection criterion as for the pulsar light curve (Section 2.5.3), we

¹⁷ <http://fermi.gsfc.nasa.gov/ssc/data/analysis/software>.

¹⁸ <http://fermi.gsfc.nasa.gov/ssc/data/access/lat/BackgroundModels.html>.

Table 4
Parameters for Four Millisecond Pulsars with Coherent Timing Solutions

	PSR J1514–4946	PSR J1658–5324	PSR J1747–4036	PSR J1902–5105
Timing parameters				
Right ascension, R.A. (J2000.0)	15 ^h 14 ^m 19 ^s .1141(1)	16 ^h 58 ^m 39 ^s .34359(9)	17 ^h 47 ^m 48 ^s .71692(3)	19 ^h 02 ^m 02 ^s .84821(9)
Declination, decl. (J2000.0)	−49°46′15″.516(5)	−53°24′07″.003(1)	−40°36′54″.773(1)	−51°05′56″.9695(8)
Proper motion in R.A., $\dot{\alpha} \cos(\delta)$ (mas yr ^{−1})	−0.3(32)	0.2(8)	−0.8(6)	−4.8(13)
Proper motion in decl., $\dot{\delta}$ (mas yr ^{−1})	−30.0(66)	4.9(23)	−4.9(16)	−4.4(16)
Spin frequency, f (Hz)	278.60300920296(5)	409.95436264371(4)	607.67753906573(2)	573.92104496683(5)
Frequency derivative, \dot{f} (Hz s ^{−1})	−1.4473(8) × 10 ^{−15}	−1.8746(6) × 10 ^{−15}	−4.8510(5) × 10 ^{−15}	−3.0301(4) × 10 ^{−15}
Epoch (MJD)	55520.0	55520.0	55520.0	55520.0
Dispersion measure, DM (pc cm ^{−3})	31.05(2)	30.81(3)	152.98(1)	36.25(1)
Orbital period, P_b (d)	1.922653523(5)	2.0118037388(9)
Projected semi-major axis, x (l-s)	1.933268(2)	1.9019570(7)
Time of ascending node, T_{asc} (MJD)	55585.8605555(3)	55162.2815604(1)
$e \sin \omega^a$, EPS1	6.453587(2) × 10 ^{−6}	5.5239429(7) × 10 ^{−6}
$e \cos \omega^a$, EPS2	8.789469(3) × 10 ^{−6}	−1.9671264(9) × 10 ^{−6}
Span of timing data (MJD)	55160–57013	55166–57057	55161–56993	55161–57014
rms timing residual (μ s)	8.3	2.9	2.4	3.8
Flux densities ^b and rotation measures				
0.8 GHz flux density, $S_{0.8}$ (mJy)	4.8	...
1.4 GHz flux density, $S_{1.4}$ (mJy)	0.17 ± 0.11 ($N = 71$)	0.7 ± 0.5 ($N = 37$)	...	1.2 ± 0.5 ($N = 69$)
1.5 GHz flux density, $S_{1.5}$ (mJy)	0.9	...
2 GHz flux density, S_2 (mJy)	0.5 ± 0.1 ($N = 28$)	...
Rotation measure, RM (rad m ^{−2})	35 ± 15	4 ± 7	−39 ± 2	...
Derived parameters ^c				
Spin period, P (ms)	3.589	2.439	1.645	1.742
Characteristic age, τ_c (10 ⁹ yr)	4.9	3.5	2.0	3.1
Spin-down luminosity, \dot{E} (10 ³⁴ erg s ^{−1})	1.0	3.0	11.3	6.7
Surface dipole magnetic field strength, B (10 ⁸ G)	2.1	1.7	1.5	1.3
Eccentricity ^a , e	(1.1 ± 0.2) × 10 ^{−5}	(5.9 ± 0.7) × 10 ^{−6}
Mass function, f_1 (M _⊙)	0.00210	0.00183
Companion mass, m_2 (M _⊙)	> 0.17	> 0.16
Spectral index ^d , α	≈ −2.5	...
Galactic longitude, l (deg)	325.25	334.87	350.21	345.65
Galactic latitude, b (deg)	6.81	−6.63	−6.41	−22.38
DM-derived distance, d (kpc)	0.9	0.9	3.4	1.2
Composite proper motion, μ (mas yr ^{−1})	30.0 ± 6.6	4.9 ± 2.2	5.0 ± 1.6	6.5 ± 1.4
Transverse velocity, V_{\perp} (km s ^{−1})	≈ 130	≈ 20	≈ 80	≈ 40

Note. — All uncertainties are reported at the 1 σ level. Numbers in parentheses represent the TEMPO2 timing uncertainties on the last digits quoted.

^a The orbital eccentricities were derived from the parameters ($e \sin \omega$, $e \cos \omega$), fitted using the TEMPO2 ELL1 binary model (Lange et al. 2001).

^b $S_{1.4}$ and S_2 values are averages and standard deviations for N detections. Individual flux densities were determined by computing the area under each pulse profile compared to its off-pulse rms, scaled using the measured system equivalent flux density at the location of the pulsar. Values for PSR J1747–4036 are from GBT observations; $S_{0.8}$ and $S_{1.5}$ are from single flux-calibrated observations (Figure 3c) and have uncertainties $\lesssim 10\%$. For one similar observation at 2 GHz, $S_2 = 0.45$ mJy.

^c The following have been used: $\tau_c = P/(2\dot{P})$, $\dot{E} = 4\pi^2 \times 10^{45} \dot{P}/P^3$ erg s^{−1}, and $B = 3.2 \times 10^{19} (P\dot{P})^{1/2}$ G, with P in s, where $P = 1/f$. The listed values of these parameters include corrections for acceleration effects (mainly due to proper motion; see Camilo et al. 1994).

^d $S_{\nu} \propto \nu^{\alpha}$, where S_{ν} is the flux density at frequency ν .

have extracted 16 gamma-ray TOAs following the method of Ray et al. (2011) and used these to extend the timing solution. The resulting parameters, including an improved measurement of the proper motion, appear in Table 5.

2.5.3. Light Curve

The gamma-ray light curve in the top panel of Figure 4, with H-test (de Jager et al. 1989; Kerr 2011b) value of 231, is a probability-weighted histogram of the photon phases. Because the probability weights w_i allow an optimal “soft” cut, no tuning of the photon selection is required, and the histogram includes all events within 2° of the pulsar position. The structure of the light curve is robust against additional background, so here, unlike in the spectral analysis, we do not apply the cut on zenith angle when the ROI is near the horizon, increasing the total number of photons by $\approx 25\%$

and slightly increasing the background level. Error bars for a bin follow the typical prescription $\sigma_j^2 = \sum_{i=1}^{N_{\gamma,j}} w_i^2$, with the sum over the $N_{\gamma,j}$ photons in the j th bin. The background level is given by $(\sum_{i=1}^{N_{\gamma}} w_i - \sum_i w_i^2)/N_{bin}$, with the sums over all N_{γ} photons in the profile and N_{bin} the total number of bins. This level, based on the spectral model, represents the expected contribution from all diffuse and background point sources. Both pulsed and unpulsed emission from the position of PSR J1903–7051 will show up as a signal in excess of this background level. However, from inspection of the light curve, it is evident that PSR J1903–7051 has no substantial unpulsed component. A slight excess may be due to an increased background over the spectral model due to the less stringent zenith cut.

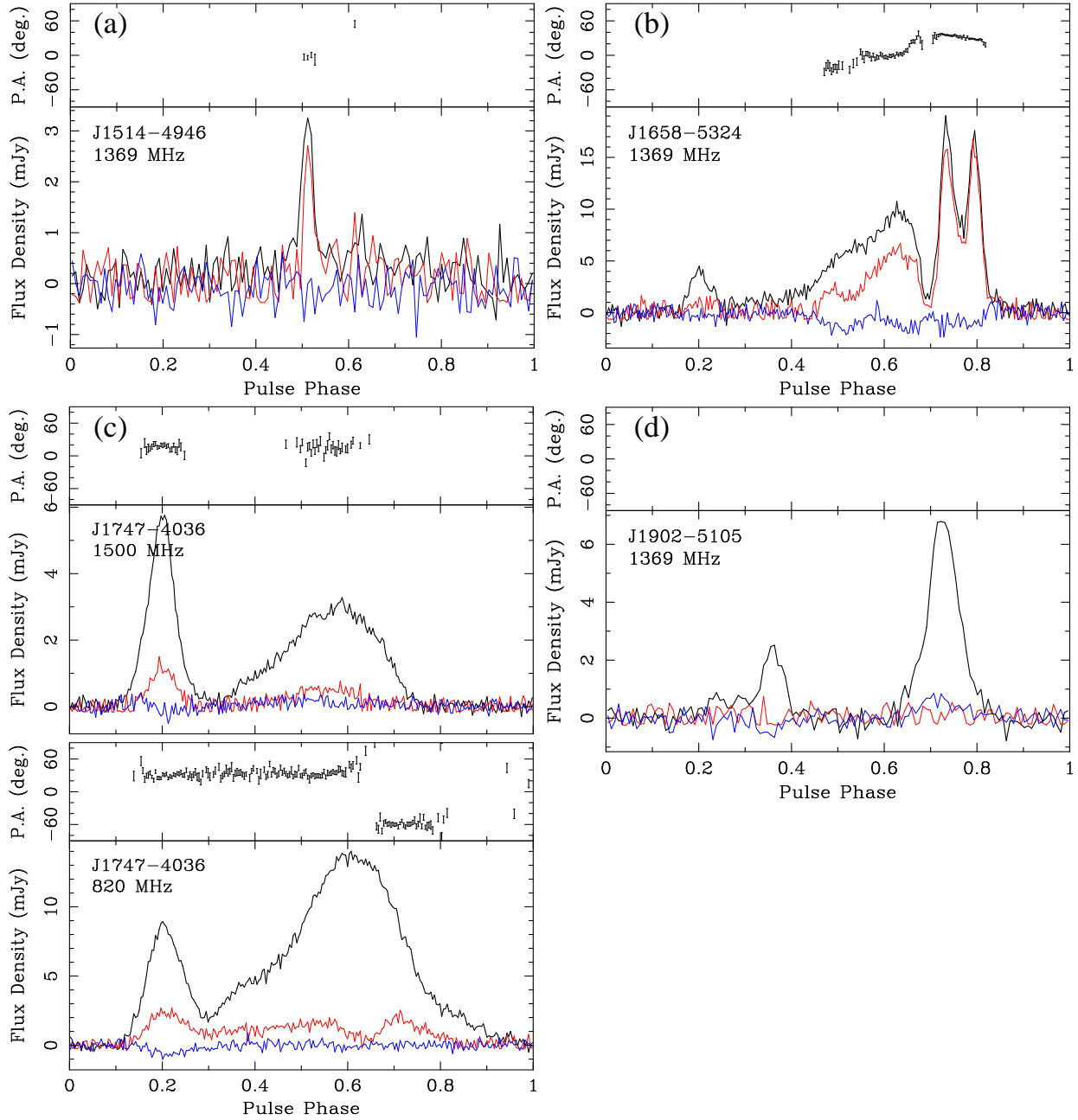


Figure 3. Polarimetric pulse profiles for PSRs J1514–4946 (a), J1658–5324 (b), J1747–4036 (c), and J1902–5105 (d). In the bottom sub-plots, the black line corresponds to total intensity, while the red and blue traces represent linear and circular polarization, respectively. In the top sub-plots, the position angle of linear polarization (P.A.) is plotted for bins in which the linear signal-to-noise ratio > 3 , corrected to the reference frame of the pulsar using the RMs listed in Table 4. PSR J1747–4036 was observed at the GBT with GUPPI (recording a bandwidth of 800 MHz at a central frequency of 1500 MHz and 200 MHz of bandwidth at 820 MHz, with the two profiles aligned by eye). All others were observed at Parkes with PDFB3 recording 256 MHz of bandwidth.

2.6. X-ray Observations

In an attempt to assist in determining accurate positions for the pulsars before timing solutions existed, we undertook X-ray observations of the fields of PSRs J1514–4946 and J1658–5324 with the ACIS-S camera on board the *Chandra X-ray Observatory* (CXO). For both observations the (then) best pulsar positions were centered on the back-illuminated S3 chip, and we analyzed the event data with the standard CIAO version 4.7 software (Fruscione et al. 2006). After excluding events outside the energy range 0.3–7.0 keV we searched the fields for any point-like X-

ray source possibly associated with the pulsars using the `celldetect` source search tool. In each case we detected a faint source $0''.3 \pm 0''.6$ away from the pulsar timing position. We name these, respectively, CXOU J151419–494615 and CXOU J165839–532406, which we identify as the pulsar counterparts on the basis of positional coincidence. Observation and source parameters are listed in Table 6.

For three other MSPs, *Swift* X-Ray Telescope (XRT) observations have been undertaken as part of a *Swift* campaign of observations of *Fermi*-LAT unassociated sources. No sources were detected at the pulsar positions. More information, in-

Table 5
Radio and Gamma-ray Parameters of PSR J1903–7051

Parameter	Value
Timing parameters	
Right ascension, R.A. (J2000.0)	19 ^h 03 ^m 38 ^s .7935(3)
Declination, decl. (J2000.0)	−70° 51′ 43″.461(2)
Proper motion in R.A., $\dot{\alpha} \cos(\delta)$ (mas yr ^{−1})	−8.8(16)
Proper motion in decl., $\dot{\delta}$ (mas yr ^{−1})	−16(2)
Spin frequency, f (Hz)	277.94006243351(8)
Frequency derivative, \dot{f} (Hz s ^{−1})	−8.06(4) × 10 ^{−16}
Epoch (MJD)	56526.0
Dispersion measure, DM (pc cm ^{−3})	19.66(1)
Orbital period, P_b (d)	11.05079833(2)
Projected semi-major axis, x (l-s)	9.938869(2)
Time of ascending node, T_{asc} (MJD)	56027.2292914(7)
$e \sin \omega$, EPS1	2.0261968(5) × 10 ^{−6}
$e \cos \omega$, EPS2	1.1855635(5) × 10 ^{−7}
Span of timing data ^a (MJD)	54760–57013
rms timing residual ^b (μ s)	12.8
Flux densities ^b and rotation measure	
1.4 GHz flux density, $S_{1.4}$ (mJy)	≈ 0.6 ($N = 9$)
3.1 GHz flux density, $S_{3.1}$ (mJy)	~ 0.14 ($N = 3$)
Rotation measure, RM (rad m ^{−2})	11 ± 24
Derived parameters ^c	
Spin period, P (ms)	3.597
Characteristic age, τ_c (10 ³ yr)	7.1
Spin-down luminosity, \dot{E} (10 ³³ erg s ^{−1})	6.8
Surface dipole magnetic field strength, B (10 ⁸ G)	1.7
Eccentricity, e	(2.0 ± 0.5) × 10 ^{−6}
Mass function, f_1 (M _⊙)	0.00863
Companion mass, m_2 (M _⊙)	> 0.28
Spectral index, α	~ −1.8
Galactic longitude, l (deg)	324.39
Galactic latitude, b (deg)	−26.51
DM-derived distance, d (kpc)	0.8
Composite proper motion, μ (mas yr ^{−1})	18.3 ± 2.0
Transverse velocity, V_{\perp} (km s ^{−1})	≈ 70
Gamma-ray parameters	
Gamma-ray–radio profile lag ^d , δ (P)	0.55 ± 0.05
Gamma-ray (> 0.1 GeV) photon index, Γ	1.90 ± 0.16
Gamma-ray cut-off energy, E_c (GeV)	7.8 ± 4.0
Photon flux (> 0.1 GeV) (10 ^{−8} cm ^{−2} s ^{−1})	1.2 ± 0.3
Energy flux (> 0.1 GeV) (10 ^{−11} erg cm ^{−2} s ^{−1})	0.9 ± 0.2

Note. — All uncertainties are reported at the 1 σ level. Numbers in parentheses represent the TEMPO2 timing uncertainties on the last digits quoted. Uncertainties for gamma-ray spectral parameters are statistical only (for a discussion of systematic errors, see Acero et al. 2015).

^a We have used both radio and gamma-ray TOAs to derive this timing solution.

^b The listed values are median flux densities for N calibrated detections. Individual $S_{1.4}$ values ranged over 0.13–1.5 mJy. In four 3.1 GHz observations we did not detect the pulsar.

^c The listed values of τ_c , \dot{E} , and B include corrections for acceleration effects.

^d This is measured from the profiles in Figure 4, with the gamma-ray profile centroid at phase $\phi = 0.27$ and the radio profile reference phase mid-way between its full observed span (0.55 < ϕ < 0.9).

cluding flux and luminosity upper limits, is given in Table 6.

All these X-ray detections and upper limits are consistent with the known distribution of MSP X-ray luminosities (e.g., Possenti et al. 2002, and references therein).

3. DISCUSSION

In our directed radio survey with the Parkes telescope of 56 unidentified *Fermi*-LAT gamma-ray sources, we detected 11

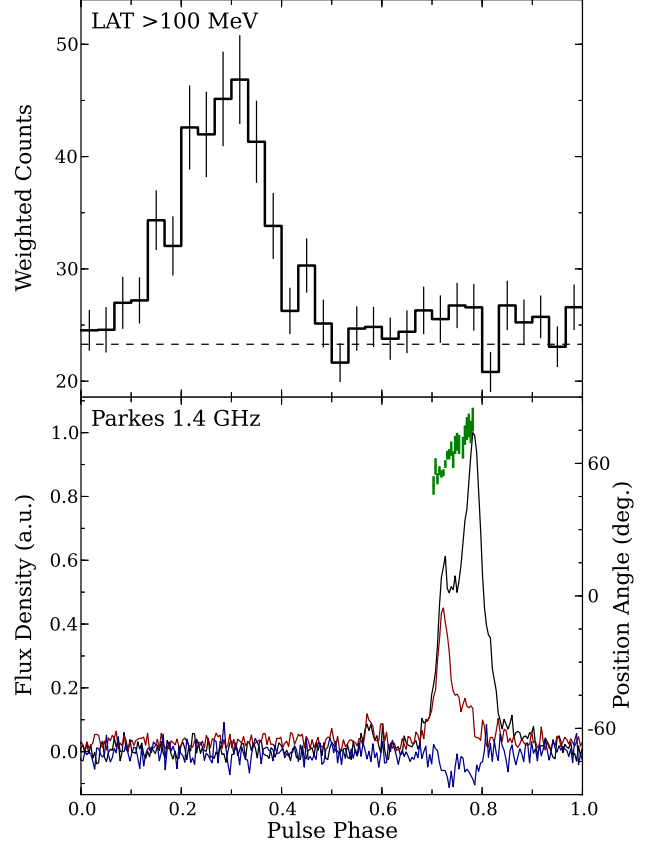


Figure 4. Gamma-ray and polarimetric radio profiles of PSR J1903–7051. *Top:* Weighted > 0.1 GeV light curve (6.5 yr of LAT data), displayed with 30 phase bins, including estimates of the error bars and the background level (see Section 2.5.3). *Bottom:* Phase-aligned Parkes 1.4 GHz pulse profile (black: total intensity; red: linear polarization; blue: circular polarization). The green error bars are centered on the position angles of linear polarization (displayed for RM = 0 with an offset of +130° for ease of view).

MSPs, 10 of them discoveries (Section 2.1).

3.1. Ten New Millisecond Pulsars

Two of the 10 new pulsars are isolated (PSRs J1658–5324 and J1747–4036; Table 4). Another five are in circular orbits ($e < 10^{-3}$) with 0.2–0.3 M_⊙ companions, likely helium-core white dwarfs (PSRs J0101–6422, J1012–4235, J1514–4946, J1902–5105, and J1903–7051; Kerr et al. 2012, and Tables 3, 4 and 5). Three of these have orbital periods of about 2 d, while the other two have periods of 11 d and 38 d. These characteristics are typical of MSPs known in the Galactic disk. The timing precision of PSR J1747–4036 is good enough that it has been added to the NANOGrav gravitational wave pulsar timing array (McLaughlin 2013).

The remaining three systems (see Table 3) are less common. PSR J0955–6150 is in a $P_b = 24$ d orbit with a $m_2 \approx 0.25$ M_⊙ companion, but with a very significant eccentricity ($e = 0.11$). It joins four Galactic MSP systems with broadly similar parameters: $0.2 < m_2 < 0.3$ M_⊙, $0.03 < e < 0.13$, $22 < P_b < 32$ d (see Antoniadis 2014; Knispel et al. 2015, and references therein). Such eccentric systems are not predicted through the standard MSP formation channels (see Phinney & Kulkarni 1994), leading to alternative scenarios (Freire & Tauris 2014; Antoniadis 2014).

Table 6
X-ray Observations of Five Millisecond Pulsars

	PSR J1514–4946	PSR J1658–5324	PSR J1747–4036	PSR J1902–5105	PSR J1903–7051
Telescope/Instrument	<i>CXO</i> /ACIS-S	<i>CXO</i> /ACIS-S	<i>Swift</i> /XRT PC	<i>Swift</i> /XRT PC	<i>Swift</i> /XRT PC
Exposure (ks)	9.9	9.9	3.3	4.2	3.2
Background-subtracted counts	9	23	< 6.6 ^a	< 12.7 ^a	< 6.6 ^a
N_{H}^{b} (10^{21} cm^{-2})	1	1	5	1	0.6
X-ray flux ^c , $f_{0.1-2.4 \text{ keV}}$ ($10^{-14} \text{ erg cm}^{-2} \text{ s}^{-1}$)	1.1	2.9	< 23	< 12 ^d	< 7
X-ray luminosity ^e , $L_{0.1-2.4 \text{ keV}}$ ($10^{-4} \dot{E}$)	1.1	0.9	< 28	< 3	< 8

Note. — A blackbody model with $kT = 0.2 \text{ keV}$ is assumed in all cases, absorbed by the indicated column density N_{H} . Considering instead a power-law spectrum with photon index $\Gamma = 2$, and calculating flux/luminosities for the 2–10 keV range, does not fundamentally alter our conclusions (Section 2.6).

^a We used $47''$ -radius extraction regions around each pulsar (90% PSF radius for XRT), and $141''$ radii to estimate backgrounds. For two sources we obtained zero background-subtracted counts, while for PSR J1902–5105 we obtained three counts. In each instance we convert to a 3σ upper limit (see Gehrels 1986).

^b Absorbing columns are estimated from the DMs according to $N_{\text{H}}(10^{21} \text{ cm}^{-2}) = 0.03 \text{ DM}$ (see He et al. 2013).

^c We used <http://heasarc.gsfc.nasa.gov/Tools/w3pimms.html> to obtain these unabsorbed flux estimates (or 3σ limits).

^d Takahashi et al. (2012) report a somewhat lower flux limit based on a 38 ks *Suzaku* XIS observation.

^e Isotropic 0.1–2.4 keV luminosities are given in terms of the acceleration-corrected values of \dot{E} , and for the DM-derived distances, listed in Tables 4 and 5.

PSR J1036–8317 is in an 8 hr orbit with a $\approx 0.16 M_{\odot}$ companion, similar to so-called “redback” systems (where outflows from $\gtrsim 0.15 M_{\odot}$ non-degenerate companions can cause irregular radio eclipses of the pulsar; e.g., D’Amico et al. 2001). Despite many observations at essentially all orbital phases, no radio eclipses have been detected. This is therefore unlikely to be a redback. More likely the companion is a white dwarf. If its distance is $\approx 1.0 \text{ kpc}$, as inferred from the DM, this could be a good target for optical studies; it may be a system similar to PSR J1012+5307, an MSP in a 14 hr orbit with a spectroscopically identified $0.16 M_{\odot}$ white dwarf (van Kerkwijk et al. 1996), or to PSR J1738+0333 (Antoniadis et al. 2012).

PSR J1946–5403 is in a 3 hr orbit with a $> 0.021 M_{\odot}$ companion. These parameters suggest a “black widow” interacting system (sub-day binaries with degenerate $\lesssim 0.05 M_{\odot}$ companions; e.g., Fruchter et al. 1988). Most such systems show radio eclipses near superior conjunction, but so far we have not detected any (when folded using the known orbital parameters, the pulsar is detected in all six data sets listed in Table 1, including two observations of superior conjunction). This could be due simply to geometry: if the actual companion mass is slightly larger than the minimum value inferred from the mass function, e.g., if $m_2 \gtrsim 0.025 M_{\odot}$, the orbital inclination angle $i \lesssim 60^{\circ}$ and we could be viewing the system relatively face-on. In any case, with a DM-derived distance of 0.9 kpc , this may also be an interesting optical target.

It seems curious that among the 10 MSPs discovered in this Parkes survey only one is in an interacting binary system (either black widow or redback), when about 50% of the 67 MSPs so far discovered in searches of unidentified LAT sources worldwide are in such systems (see Roberts 2013). For instance, in a recent survey at Arecibo, five of six MSPs discovered are either black widows or redbacks (H. T. Cromartie et al. 2015, in preparation). However, the Arecibo searches have integration times of $T = 15 \text{ min}$, which are far more suitable for the discovery of few-hour binaries than the 1 hr Parkes integrations: the maximum accelerations probed by our searches scale as T^{-2} . At the GBT, where half of these 67 MSPs were discovered, typical integration times are 30–45 min (e.g., Ransom et al. 2011, P. Bangale et al. 2015, in preparation). In any case, the pulsars that we did not detect unbiasedly in every one of our Parkes survey observations are the two sub-day binaries (Table 1), at least in part due to large and rapidly changing orbital acceleration (cf. Figure 1).

3.2. Six New Gamma-ray Millisecond Pulsars

Radio timing observations since 2009 have yielded rotational ephemerides for 43 of the 67 MSPs discovered in LAT-guided searches. Of these, 39 are now confirmed as gamma-ray MSPs (the other four are unrelated to the LAT sources; e.g., Keith et al. 2011), including the six discovered in our Parkes survey for which we already have timing solutions. In this paper we have for the first time presented the ephemerides and polarimetry for five of these MSPs, and gamma-ray properties for PSR J1903–7051. In some cases these results add to our understanding of the pulsars summarized in the second LAT catalog of gamma-ray pulsars (2PC; Abdo et al. 2013).

For PSR J1903–7051, the radio peak leads the gamma-ray profile by $\delta \approx 0.5 P$. Other pulsars with such values of δ have gamma-ray profiles composed of only one peak (2PC), which is also the case for PSR J1903–7051 (Figure 4). This is one of the few MSPs for which spectral curvature (deviation from a power-law spectrum) is not apparent even with 4 yr of LAT data (Table 2). Our spectral fits to 6.5 yr of data yield the largest cut-off energy of any pulsar, even if with large uncertainty: $E_c = (7.8 \pm 4.0) \text{ GeV}$ (Table 5; see also Figure 5f). The MSPs with the next largest values of E_c are also from our Parkes sample: PSRs J1747–4036 and J1514–4946 (2PC).

With our proper motion measurement for PSR J1514–4946 (Table 4), its intrinsic \dot{E} is 1.6 times smaller than previously thought. Its computed gamma-ray efficiency, already high in 2PC (30%), now increases to 50%. As usual this assumes a geometry-dependent beaming correction of $f_{\Omega} = 1$ (see 2PC for definition), i.e., assuming isotropic emission. Perhaps for PSR J1514–4946, $f_{\Omega} \ll 1$. Or maybe its DM-derived distance of 0.9 kpc is an overestimate (its nominal transverse velocity is the largest of those listed in Tables 4 and 5, although it is not unusually large for an MSP; e.g., Gonzalez et al. 2011).

PSR J1747–4036 is notable in several respects. Spectral curvature is not apparent in the 3FGL catalog (see Table 2). Its \dot{E} is large (fourth highest among the 2PC MSP sample). Its nominal distance (Table 4) is also among the largest in the 2PC MSP sample, and it is a relatively faint gamma-ray source (10σ in 3FGL; Table 2). If it had a typical \dot{E} at that distance presumably it would not be a detectable LAT pulsar. This large \dot{E} ultimately is due to its very short spin period (third shortest among disk MSPs). While PSR J1747–4036 may be somewhat extreme in this regard, it does appear that LAT-detected MSPs are a smaller- P , higher- \dot{E} population than

radio-selected MSPs (Ray et al. 2012). In our Parkes sample, PSRs J1902–5105 and J0955–6150 (the latter apparently quite distant) are also short-period MSPs, with $P < 2$ ms.

PSR J1902–5105 is one of only six MSPs known with phase-aligned gamma-ray and radio light curves (2PC). This points to emission that is either extended, and caustic in nature, or originates near the neutron star surface (Venter et al. 2012). In order to constrain their emission and viewing geometry, Johnson et al. (2014) have jointly modeled the gamma-ray and radio profiles of 40 LAT-detected MSPs. They fit gamma-ray light curves using standard outer magnetosphere gap (OG) and two-pole caustic (TPC) geometric models assuming a vacuum retarded dipole magnetic field. For PSR J1902–5105, Johnson et al. (2014) consider altitude-limited (al) versions of the standard models as well as a low-altitude slot gap model (laSG). They find that all three models match the gamma-ray and radio profiles fairly well. However, the complete lack of polarization that we observe (Figure 3d) strongly favors the alTPC and alOG models, where high-altitude caustics are predicted to have a strong depolarizing effect (Dyks et al. 2004), over the laSG model, where one expects non-zero polarization from near-surface emission.

For PSR J1514–4946, the high level of observed linear polarization and modest P.A. swing (Figure 3a and Section 2.4) suggest we are viewing the edge of a cone beam at relatively low altitude. For PSR J1658–5324, the very high level of linear polarization suggests that at least some components originate at relatively low altitude (the small peak with low polarization, which might also originate from the opposite pole, could be a high-altitude caustic; Figure 3b). PSR J1747–4036 has a very unusual polarization pattern (Figure 3c), which does not fit either standard radio core/cone or high-altitude caustic emission models. For these MSPs, Johnson et al. (2014) find models that plausibly match the gamma-ray light curves, but the radio profiles are not well reproduced.

3.3. Survey Statistics

Our survey of unidentified LAT sources had a success rate of 20% (11 MSPs detected unbiasedly in 56 sources searched; Section 2.1), despite significant selection effects (Section 2.2). This is very encouraging — a substantial number of unidentified LAT sources contain previously unknown MSPs that can be detected at Parkes, and our source selection criteria have allowed us to target them with satisfactory efficiency. However, comparing the initial segment of the survey (Section 2.1.1) with the latter portion (Section 2.1.2) reveals a drop in efficiency: we had to search 3.5 times as many sources in 2012, for twice as long in the aggregate, to discover as many pulsars as earlier on.

Since our observations, another six pulsars have been discovered in these very same sources: four via direct pulsation searches of the gamma-ray photons, one of which was subsequently detected as a very faint radio source with the GBT (the others might be significantly affected by scintillation, or perhaps they may yet prove to be gamma-ray-only pulsars); one at the Giant Metrewave Radio Telescope (GMRT) at a lower frequency than at Parkes (perhaps the Parkes non-detections reflect a steep radio spectrum); and one that is a transient radio source — not active when we did our Parkes searches, but now detectable there (see notes l–o in Table 2). Considering these additional detections, a full 10 of the original 14 targets of our survey are now known to contain pulsars! This reflects superb source selection criteria for those targets. Why has the success rate decreased since then? The original (1FGL-

based) sources were brighter in gamma rays, allowing for relatively unambiguous determination of spectral characteristics, on which we based our target selection. There might be secondary effects related to this: e.g., the brighter 1FGL-based targets might be nearer to the Earth on average, and any associated radio pulsars could then also be brighter on average, although we do not see such an effect among our small sample of *detected* MSPs.

3.4. Spectral Characteristics of LAT Pulsars

Now that the third catalog of LAT sources is in hand, based on substantially more data and a much better understanding of the instrument and background than was available earlier, we can usefully revisit our 56 sources and the MSPs found amid them. In Table 2 we have summarized some properties of these sources as obtained from the 3FGL catalog. Given that gamma-ray pulsars typically have exponentially cut-off power-law spectra (Abdo et al. 2013), by contrast to power-law spectra for AGN, it is not surprising that the spectral curvature gleaned from 3FGL correlates well with gamma-ray pulsars: of the 12 pulsars with known gamma-ray pulsations listed in Table 2 (the eight classified as “PSR,” as well as J1035.7–6720, J1227.9–4854, J1624.2–4041, and J1744.1–7619), 10 display significant curvature according to 3FGL (Curve $> 4\sigma$; Table 2). However, two other established gamma-ray MSPs (PSRs J1747–4036 and J1903–7051, reported here) show no curvature, according to 3FGL (Curve $< 3\sigma$). Now that 170 gamma-ray pulsars are known, it is to be expected that some may depart from the norm. In addition, “Curve” in 3FGL tests against a log-parabolic spectral model, which may not be a good proxy for testing against exponentially cut-off power laws, especially when the source is not very bright or the background is problematic (as it happens, these two MSPs are the faintest in gamma rays of the 12 under consideration; see “Sig” in Table 2). Thus, in considering whether a particular 3FGL source is a good pulsar candidate, we should do more than simply look for significant cataloged curvature.

3.5. Spectral Classification of Unidentified LAT Sources

Flux information is available from the 3FGL pipeline processing in five energy bins (two within 0.1–1 GeV, two within 1–10 GeV, and one for 10–100 GeV). After familiarizing ourselves with how known gamma-ray pulsars (and control sources) appear in five-bin spectra by visual inspection of many 3FGL plots, we have classified the 56 target sources of our Parkes survey according to a heuristic ranking scheme that we describe next.

We qualitatively assess the likelihood of a source being a pulsar. According to this scheme, a classification of “1” denotes near certainty of being a pulsar; “2” is less conclusive but quite plausible; “3” is a poorer pulsar candidate; “4” is very likely not a pulsar; “5” is not a pulsar.

These classifications are based on combinations of the following spectral characteristics (both are listed for each source in Table 2): strong energy cutoff (c); parabolic (peak at center energies, p); flat or rising spectrum at < 1 GeV (r) — c, p, r are “positive” features leading to higher likelihood of a source being a pulsar (for examples, see Figure 5c and e). Power law (l); variability (v); monotonically decreasing (d) or increasing (i); excess high energy emission (flat or rising spectrum; h) — l, v, d, i, h are “negative” features, not ordinarily associated with pulsars (see Figure 5a and d). Capitalization means that

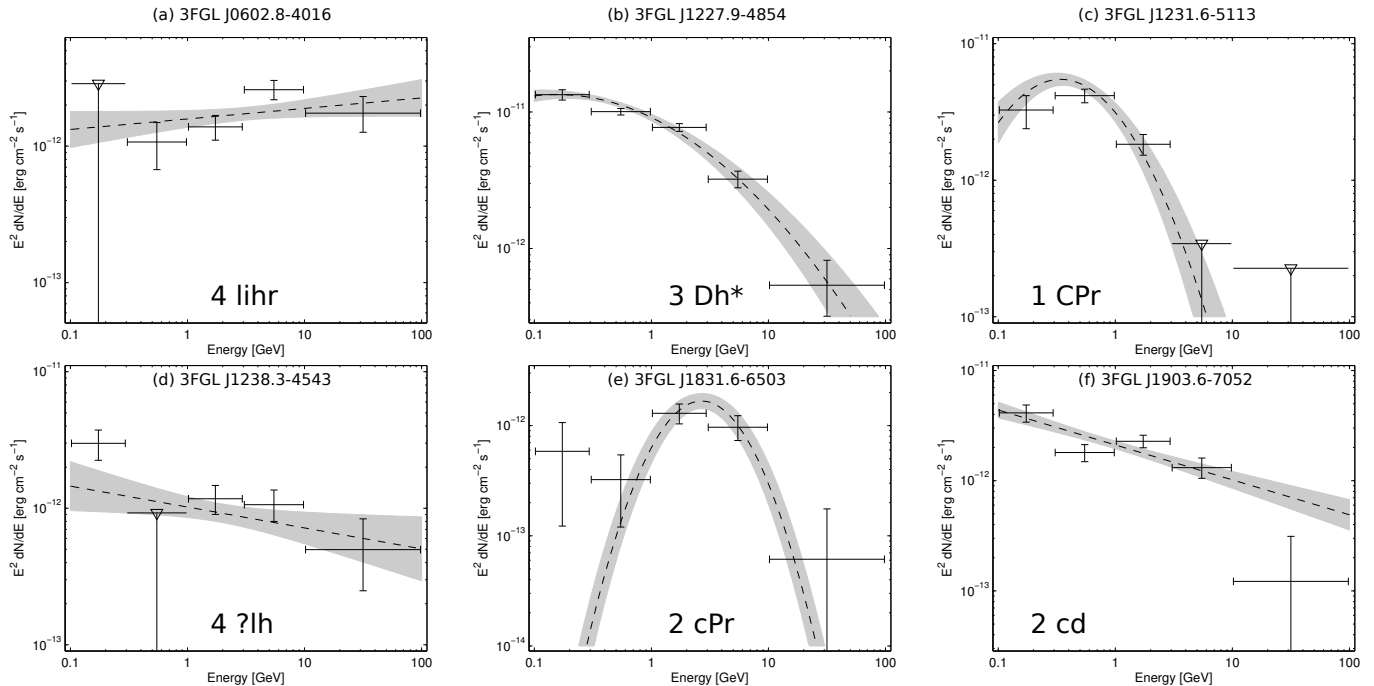


Figure 5. Examples of spectral classification of unidentified *Fermi*-LAT sources with a view towards identifying pulsar candidates. The panels show the spectral energy distribution (SED) from the 3FGL analysis (Acero et al. 2015), with the dashed lines/gray bands indicating the best-fit model SED (either a power law or a curved log-parabolic spectrum) and its uncertainties. Discrepancies between the spectral measurements and the model indicate that the fit may be unreliable. Our classifications (1–5) and qualitative spectral characteristics that underlie them are described in Section 3.5. The full list of 56 classified sources searched in our Parkes radio survey is given in Table 2. **(a)** An example of a poor pulsar candidate, consistent with a power law (l), with both high-energy emission (h) and an AGN association; **(b)** an example of an atypical pulsar spectrum, now associated with the state-changing MSP J1227–4853; **(c)** an excellent candidate with a strong cutoff (C), a spectrum slightly more peaked than that of the typical pulsar (P), and rising at < 1 GeV (r); **(d)** a poor candidate spectrum with both high-energy emission (h) and unreliable spectral points (?); **(e)** a good candidate with an unusually peaked spectrum (P); **(f)** a decent candidate with evidence for a cutoff (c) but an unusually steep low-energy spectrum, monotonically decreasing (d); now known to be PSR J1903–7051 (this work; e.g., see Table 5 and top panel of Figure 4).

the features are more certain, except for p/P which indicates the sharpness of the parabola. A “?” indicates poor spectral quality, increasing uncertainty in classification. An asterisk represents an odd spectrum with “banana” shape to high energy (see Figure 5b). In Figure 5 we show 3FGL spectral plots for six of our Parkes targets that illustrate the features described above.

Sixteen of our 56 sources are classified as 5 or 4 (or 3 with a blazar association), and we regard them as no longer viable pulsar candidates.

Of the 12 known gamma-ray pulsars in Table 2, nine are classified as 1 and two others (already noted in Section 3.4 as not curved in 3FGL) as 2. The one confirmed gamma-ray MSP classified as a 3, PSR J1227–4853, is a spectral outlier (Figure 5b). In a rare state-changing binary system, it is borderline variable within 3FGL, and recently displayed significant variability (see Johnson et al. 2015). This and its sister system J1023+0038 (Stappers et al. 2014), as well as the young pulsar J2021+4026 (Allafort et al. 2013), are counterexamples to the usual assumption that pulsars are steady gamma-ray emitters. Of the other five MSPs known in Table 2 (none of which has yet a reported long-term timing solution or detected gamma-ray pulsations), one is classified as 1, one as 2, and three as 3. Based on prior statistics, we expect that most, perhaps all, of these five MSPs will eventually be established as gamma-ray pulsars. That most have a relatively poor classification in our scheme likely reflects their faintness (three, all discovered in our survey, have 3FGL significance of 6.6 – 8.8σ), or location close to the Galactic plane

(PSR J1536–4948 is at $b = 4.8^\circ$).

3.6. Further Searches of LAT Sources

Following from the discussion in Section 3.5, while we certainly recommend additional searches first of the “1” sources that remain without coincident pulsars (of which there are seven in Table 2), followed by the “2” sources (nine in Table 2), the “3” sources (seven in Table 2) are also reasonable candidates for further searches¹⁹. Among these 23 sources, two are coincident with globular clusters that currently have no known pulsars, and a population of MSPs in those clusters is a plausible origin for the gamma-ray emission. We expect further MSP discoveries among these 23 targets: while the largest offset between our optimized search and the 3FGL positions is $3'$, which is not very large compared to the $7/2$ half-width at half-maximum Parkes beam, many promising targets have not been searched enough to counter the selection effects presented in Section 2.2 — e.g., four of the seven “1” sources have been searched at Parkes only once or twice at locations not far from their 3FGL positions (see Table 2). In addition, in the near future we intend to re-analyze our existing data sets with “jerk searches,” i.e., accounting for changing accelerations that are relevant for short orbital periods (cf. Figure 1).

After all such searches are done, it remains a possibility that through a combination of faintness and extreme orbital and spin parameters, some of those promising LAT sources could

¹⁹ One of the “2” sources, 3FGL J1417.5–4402, has recently been reported to be a binary system currently with an accretion disk (Strader et al. 2015).

still harbor undetected radio MSPs beamed towards the Earth. It is also possible that some of these sources may be MSPs that are detectable only via their gamma-ray emission, although this fraction is known to be small (e.g., Romani 2012).

We are grateful to the wonderful staff at the Parkes telescope for their role in making it such a fine research instrument. We thank in particular the friends of the analog filter-bank system, used to discover more than 1000 pulsars, who staved off its demise long enough to allow the completion of this work. We thank Willem van Straten and Paul Demorest for their help with PSRCHIVE. The Parkes Observatory is part of the Australia Telescope, which is funded by the Commonwealth of Australia for operation as a National Facility managed by CSIRO.

The National Radio Astronomy Observatory is a facility of the National Science Foundation operated under cooperative agreement by Associated Universities, Inc.

The *Fermi* LAT Collaboration acknowledges generous ongoing support from a number of agencies and institutes that have supported both the development and the operation of the LAT as well as scientific data analysis. These include the National Aeronautics and Space Administration (NASA) and the Department of Energy in the United States, the Commissariat à l’Energie Atomique and the Centre National de la Recherche Scientifique / Institut National de Physique Nucléaire et de Physique des Particules in France, the Agenzia Spaziale Italiana and the Istituto Nazionale di Fisica Nucleare in Italy, the Ministry of Education, Culture, Sports, Science and Technology (MEXT), High Energy Accelerator Research Organization (KEK) and Japan Aerospace Exploration Agency (JAXA) in Japan, and the K. A. Wallenberg Foundation, the Swedish Research Council and the Swedish National Space Board in Sweden.

Facilities: Parkes (PMDAQ, PDFB), GBT (GUPPI), Fermi (LAT), CXO (ACIS-S), Swift (XRT)

REFERENCES

- Abdo, A. A., Ackermann, M., Ajello, M., et al. 2009a, *Science*, 325, 848
 —. 2009b, *Science*, 325, 840
 —. 2010a, *ApJS*, 188, 405
 —. 2010b, *ApJS*, 187, 460
 Abdo, A. A., Ajello, M., Allafort, A., et al. 2013, *ApJS*, 208, 17
 Acero, F., Ackermann, M., Ajello, M., et al. 2015, *ApJS*, 218, 23
 Allafort, A., Baldini, L., Ballet, J., et al. 2013, *ApJ*, 777, L2
 Alpar, M. A., Cheng, A. F., Ruderman, M. A., & Shaham, J. 1982, *Nature*, 300, 728
 Antoniadis, J. 2014, *ApJ*, 797, L24
 Antoniadis, J., van Kerkwijk, M. H., Koester, D., et al. 2012, *MNRAS*, 423, 3316
 Atwood, W. B., Abdo, A. A., Ackermann, M., et al. 2009, *ApJ*, 697, 1071
 Bagchi, M., Lorimer, D. R., & Wolfe, S. 2013, *MNRAS*, 432, 1303
 Barr, E. D., Guillemot, L., Champion, D. J., et al. 2013, *MNRAS*, 429, 1633
 Camilo, F., Thorsett, S. E., & Kulkarni, S. R. 1994, *ApJ*, 421, L15
 Cognard, I., Guillemot, L., Johnson, T. J., et al. 2011, *ApJ*, 732, 47
 Cordes, J. M., & Lazio, T. J. W. 2002, preprint (arXiv:astro-ph/0207156)
 Dai, S., Hobbs, G., Manchester, R. N., et al. 2015, *MNRAS*, 449, 3223
 D’Amico, N., Possenti, A., Manchester, R. N., et al. 2001, *ApJ*, 561, L89
 de Jager, O. C., Raubenheimer, B. C., & Swanepoel, J. W. H. 1989, *A&A*, 221, 180
 Dyks, J., Harding, A. K., & Rudak, B. 2004, *ApJ*, 606, 1125
 Freire, P. C., Kramer, M., & Lyne, A. G. 2001, *MNRAS*, 322, 885
 Freire, P. C. C., & Tauris, T. M. 2014, *MNRAS*, 438, L86
 Fruchter, A. S., Stinebring, D. R., & Taylor, J. H. 1988, *Nature*, 333, 237
 Fruscione, A., McDowell, J. C., Allen, G. E., et al. 2006, in *Society of Photo-Optical Instrumentation Engineers (SPIE) Conference Series*, 6270
 Gehrels, N. 1986, *ApJ*, 303, 336
 Gonzalez, M. E., Stairs, I. H., Ferdman, R. D., et al. 2011, *ApJ*, 743, 102
 He, C., Ng, C.-Y., & Kaspi, V. M. 2013, *ApJ*, 768, 64
 Hessels, J. W. T., Roberts, M. S. E., McLaughlin, M. A., et al. 2011, in *AIP Conf. Series*, Vol. 1357, *Radio Pulsars*, ed. M. Burgay, N. D’Amico, P. Esposito, A. Pellizzoni, & A. Possenti, 40–43
 Hobbs, G. B., Edwards, R. T., & Manchester, R. N. 2006, *MNRAS*, 369, 655
 Hotan, A. W., van Straten, W., & Manchester, R. N. 2004, *PASA*, 21, 302
 Johnson, T. J., Venter, C., Harding, A. K., et al. 2014, *ApJS*, 213, 6
 Johnson, T. J., Ray, P. S., Roy, J., et al. 2015, *ApJ*, 806, 91
 Johnston, H. M., & Kulkarni, S. R. 1991, *ApJ*, 368, 504
 Johnston, S., Nicastro, L., & Koribalski, B. 1998, *MNRAS*, 297, 108
 Keith, M. J., Johnston, S., Ray, P. S., et al. 2011, *MNRAS*, 414, 1292
 Kerr, M. 2011a, PhD thesis, University of Washington, arXiv:1101.6072
 —. 2011b, *ApJ*, 732, 38
 Kerr, M., Camilo, F., Johnson, T. J., et al. 2012, *ApJ*, 748, L2
 Knispel, B., Lyne, A. G., Stappers, B. W., et al. 2015, *ApJ*, 806, 140
 Lange, C., Camilo, F., Wex, N., et al. 2001, *MNRAS*, 326, 274
 Levin, L., Bailes, M., Barsdell, B. R., et al. 2013, *MNRAS*, 434, 1387
 Lorimer, D. R., & Kramer, M. 2005, *Handbook of Pulsar Astronomy* (Cambridge University Press)
 McLaughlin, M. A. 2013, *Classical and Quantum Gravity*, 30, 224008
 Nicastro, L., Nigro, F., D’Amico, N., Lumiella, V., & Johnston, S. 2001, *A&A*, 368, 1055
 Nolan, P. L., Abdo, A. A., Ackermann, M., et al. 2012, *ApJS*, 199, 31
 Phinney, E. S., & Kulkarni, S. R. 1994, *Ann. Rev. Astr. Ap.*, 32, 591
 Pletsch, H. J., Guillemot, L., Fehrmann, H., et al. 2012a, *Science*, 338, 1314
 Pletsch, H. J., Guillemot, L., Allen, B., et al. 2012b, *ApJ*, 744, 105
 Possenti, A., Cerutti, R., Colpi, M., & Mereghetti, S. 2002, *A&A*, 387, 993
 Radhakrishnan, V., & Cooke, D. J. 1969, *Astrophys. Lett.*, 3, 225
 Ransom, S. M. 2001, PhD thesis, Harvard University
 Ransom, S. M., Eikenberry, S. S., & Middleditch, J. 2002, *AJ*, 124, 1788
 Ransom, S. M., Ray, P. S., Camilo, F., et al. 2011, *ApJ*, 727, L16
 Ray, P. S., Kerr, M., Parent, D., et al. 2011, *ApJS*, 194, 17
 Ray, P. S., Abdo, A. A., Parent, D., et al. 2012, eConf C110509, arXiv:1205.3089
 Ray, P. S., Ransom, S. M., Cheung, C. C., et al. 2013, *ApJ*, 763, L13
 Rickett, B. J. 1990, *Ann. Rev. Astr. Ap.*, 28, 561
 Roberts, M. S. E. 2013, in *IAU Symposium*, Vol. 291, ed. J. van Leeuwen, 127–132
 Romani, R. W. 2012, *ApJ*, 754, L25
 Roy, J., Ray, P. S., Bhattacharyya, B., et al. 2015, *ApJ*, 800, L12
 Stappers, B. W., Archibald, A. M., Hessels, J. W. T., et al. 2014, *ApJ*, 790, 39
 Strader, J., Chomiuk, L., Cheung, C. C., et al. 2015, *ApJ*, 804, L12
 Takahashi, Y., Kataoka, J., Nakamori, T., et al. 2012, *ApJ*, 747, 64
 Thorsett, S. E., & Chakrabarty, D. 1999, *ApJ*, 512, 288
 van Kerkwijk, M. H., Bergeron, P., & Kulkarni, S. R. 1996, *ApJ*, 467, L89
 Venter, C., Johnson, T. J., & Harding, A. K. 2012, *ApJ*, 744, 34
 Yan, W. M., Manchester, R. N., van Straten, W., et al. 2011, *MNRAS*, 414, 2087